RSC Advances

PAPER

View Article Online
View Journal | View Issue

Check for updates

Cite this: *RSC Adv.*, 2020, **10**, 3084

Acetaldehyde-modified-cystine functionalized Zr-MOFs for pH/GSH dual-responsive drug delivery and selective visualization of GSH in living cells†

Caixue Lin, ‡[a] Hailu He,‡[a] Yongqi Zhang,[a] Mingyue Xu,[a] Feng Tian,[a] Ling Li *[ab] and Yingxi Wang[a]

In recent years, the construction of drug carriers that integrate diagnosis and treatment has become a new trend. In this article, a metal–organic framework (Zr-MOF) was synthesized and functionalized using acetaldehyde-modified-cystine (AMC) to form the functional drug carrier Zr-MOF/AMC which could be used to determine the concentration of glutathione (GSH) for cancer diagnosis, and to achieve pH/GSH dual-responsive release of methotrexate (MTX) for cancer therapy. The cleavage of the AMC disulfide bond by GSH generates two fluorescent molecules that produce strongly enhanced fluorescence, and the intensity is proportional to the GSH concentration. The green fluorescence of Zr-MOF/AMC in cancer cells proves that it can be applied in cell imaging to detect abnormal GSH concentrations for early diagnosis. In addition, MTX loaded on the Zr-MOF/AMC is released by the cleavage of the –S–S– and –C=N– bonds at the high GSH concentration and low pH in cancer cells. This dual-responsive drug release helps to deliver drugs to cancer cells more precisely. All the experiments suggest that this novel type of pH/GSH dual-responsive Zr-MOF/AMC nanoparticle may serve as a new drug delivery system for cancer diagnosis and treatment.

Received 25th July 2019
Accepted 4th December 2019

DOI: 10.1039/c9ra05741b

rsc.li/rsc-advances

Open Access Article. Published on 17 January 2020. Downloaded on 12/9/2025 4:51:02 AM.
This article is licensed under a Creative Commons Attribution-NonCommercial 3.0 Unported Licence.

1 Introduction

Cancer is one of the most life-threatening diseases.[1] The construction of smart drug carriers that integrate diagnosis and drug release has become a research trend. As the microenvironment of cancer cells is different from that of normal cells, the determination of relative concentrations of substances in the cellular microenvironment can help with early cancer diagnosis. Glutathione (GSH) is a tripeptide containing a thiol group, an amino group and a γ-amide bond, consisting mainly of glutamic acid, cysteine and glycine.[2] It is an important regulator of metabolism in cells: it can not only clear peroxide and other free radicals in the body, promote liver enzyme activity, and detoxify and maintain erythrocyte membrane integrity and other functions, but it also maintains DNA biosynthesis and various physiological functions such as cellular immunity.[3,4] Fluctuations in the concentration of GSH can cause many diseases, such as leukopenia, cancer, psoriasis and liver damage, *etc.*[5,6] Because the concentration of GSH (~20 mM) in cancer cells is very different from that in normal cells (~5 mM), the early diagnosis of cancer by detecting GSH levels has attracted the attention of many researchers. For example, Yi and co-authors reported a dual-mode nanosensor with both a colorimetric and a fluorometric readout based on carbon quantum dots and gold nanoparticles for the discriminative detection of GSH over Cys/Hcy, and this allowed the detection of GSH at concentrations of as low as 50 nM.[7] Cheng and co-authors reported bimetallic oxide MnMoOX nanorods as an intelligent nanoprobe for *in vivo* GSH detection *via* photoacoustic (PA) imaging. The obtained MnMoOX nanoprobe, which had no near-infrared (NIR) absorption in the absence of GSH, exhibited strong GSH-responsive NIR absorbance, enabling the detection of GSH by PA imaging.[8] However, although such probes can determine cancer markers, it has been difficult to achieve cancer treatment at the same time.

At present, chemotherapy remains one of the most important cancer therapies.[9] Based on the different pH value and GSH concentration of cancer cells compared with normal cells, a large number of pH-responsive and GSH-responsive drug carriers have been synthesized to deliver drugs to cancer cells, and facilitate the reduction of side effects in normal cells.[10] Therefore, it is hoped that a smart drug carrier that integrates diagnosis and treatment can be obtained through the combination of GSH determination and drug delivery.

[a]*Hubei Collaborative Innovation Center for Advanced Organic Chemical Materials, Ministry-of-Education Key Laboratory for the Synthesis and Application of Organic Function Molecules, Hubei University, 430062, People's Republic of China. E-mail: waitingll@yahoo.com*

[b]*ARC Centre of Excellence in Convergent Bio-Nano Science and Technology, Brisbane, Qld 4072, Australia*

† Electronic supplementary information (ESI) available. See DOI: 10.1039/c9ra05741b

‡ These authors contributed equally to this work.

This journal is © The Royal Society of Chemistry 2020

Open Access Article. Published on 17 January 2020. Downloaded on 12/9/2025 4:51:02 AM.
This article is licensed under a Creative Commons Attribution-NonCommercial 3.0 Unported Licence.

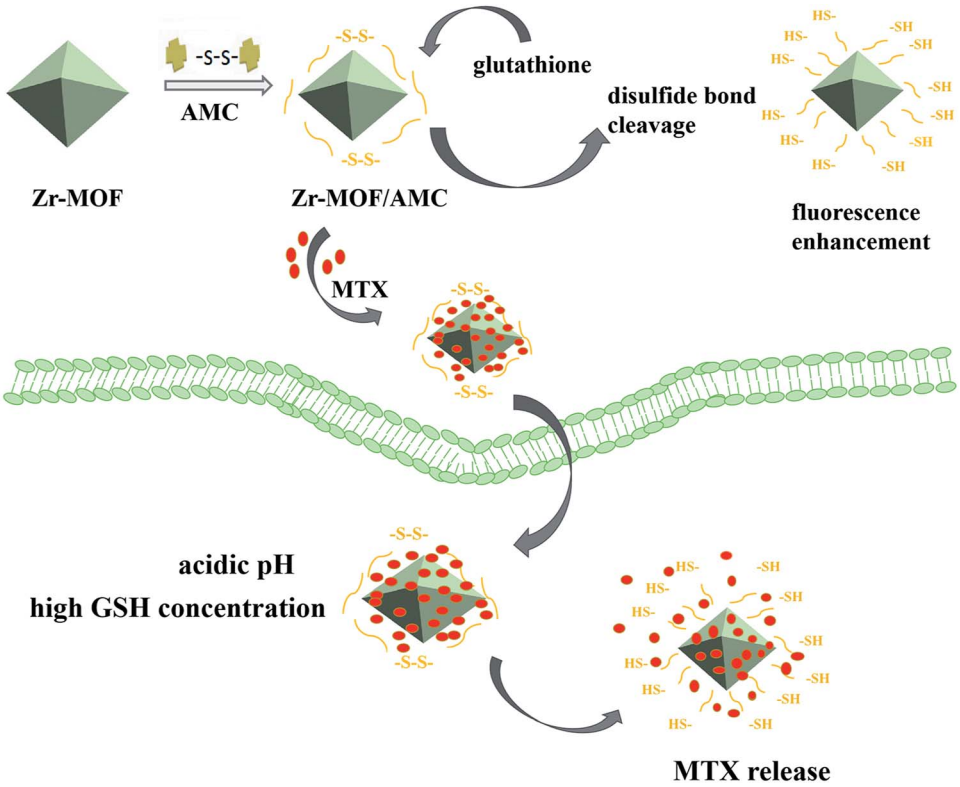

Scheme 1 Schematic illustration of the synthetic procedure for Zr-MOF/AMC/MTX and the proposed mechanisms by which Zr-MOF/AMC nanoparticles act as a GSH probe and dual-responsive drug carrier.

Metal–organic frameworks (MOFs) are a new class of porous framework materials, which have been extensively investigated for drug delivery[11,12] due to their high drug-carrying capacity, ease of modification, good biodegradability and good biocompatibility.[13,14] Acetaldehyde-modified-cystine (AMC) is a self-fluorescing substance that is induced by the n–π* transition of the two –C═N– bonds.[15] When the disulfide bond in AMC encounters a thiol in GSH, there is a thiol–disulfide exchange reaction and fluorescence enhancement due to disulfide bond cleavage. This offers highly sensitive and selective detection of GSH.[16] Inspired by these observations, we used Zr-MOF as a drug-loading system, and modified it with AMC to achieve the early detection of tumors and the controllable release of drugs. The preparation of the nanocarrier for GSH detection and intracellular pH/GSH triggered release, as illustrated in Scheme 1. The AMC is coated on the surface of the Zr-MOF through an amide reaction to form a stable hybrid Zr-MOF/AMC. Methotrexate (MTX), an anti-folate antitumor drug that inhibits the growth and reproduction of tumor cells,[17] is loaded into Zr-MOF/AMC to enable dual-responsive drug release. The –S–S– bond breaks to promote the drug release at high concentrations of GSH, and –C═N– bonds hydrolyze and partially break under acidic conditions.[18,19] Thus the carrier can be used for precisely delivering drugs to cancer cells. In addition, at high GSH concentrations, the enhanced fluorescence of Zr-MOF/AMC can be used for cell imaging and diagnosis. As a result, Zr-MOF/AMC can serve as a potential platform for both intracellular GSH imaging and pH/GSH dual-responsive drug release.

2 Experimental

2.1 Chemicals and reagents

Acetaldehyde, cystine, HCl (36.0–38.0%), *N*,*N*-dimethylformamide, methotrexate (MTX), glutathione (GSH), *N*-hydroxysuccinimide, *N*-ethylmaleimide and 1-ethyl-3-(3-dimethylaminopropyl)carbodiimide were purchased from Aladdin Industrial Corporation. Zirconium chloride, 2-aminoterephthalic acid, acetic acid and sodium hydroxide were purchased from Sinopharm (Shanghai) Chemical Reagent Co., Ltd., China. All other chemicals used in this work were of analytical grade, were obtained from commercial suppliers, and were used without further purification unless otherwise noted. Fresh double-distilled water was used in all experiments.

2.2 Instruments

Powder X-ray diffraction (XRD) patterns were obtained using a D8 Advance X-ray diffractometer (Bruker Company, Germany). Fourier transform infrared (FT-IR) spectra were obtained using a Spectrum One FT-IR spectrophotometer (PerkinElmer, USA) at room temperature. Transmission electron microscopy (TEM) images were obtained on a Tecnai G20 microscope (FEI, America). Morphologies of the samples were observed by scanning electron microscopy (SEM) on a JSM6510LV scanning

Open Access Article. Published on 17 January 2020. Downloaded on 12/9/2025 4:51:02 AM.
This article is licensed under a Creative Commons Attribution-NonCommercial 3.0 Unported Licence.

electron microscope (JEOL, Japan). The fluorescence measurements were recorded on an LS55 fluorescence spectrometer (PerkinElmer, America).

2.3 Synthesis methods

Synthesis of Zr-MOF. Zr-MOF was prepared following a previously reported procedure.[20] Typically, $ZrCl_4$ (0.0745 g, 0.3197 mmol) and 2-aminoterephthalate (0.072 g, 0.3978 mmol) were dissolved in anhydrous *N*,*N*-dimethylformamide (50 mL) at room temperature. After that, acetic acid (5.5 mL) was added in drops. The obtained mixture was stirred at room temperature for 30 min, then transferred to a 30 mL Teflon liner and heated at 120 °C for 24 h. After aging, precipitates were collected by centrifugation and washed with *N*,*N*-dimethylformamide and ethanol. The product was obtained after drying under vacuum.

Synthesis of AMC. Briefly, 1 g of cystine was dissolved in 50 mL of deionized water and the pH of the mixture was adjusted to 10 with 0.1 mol L^{-1} NaOH. Then 2.0 mL of acetaldehyde was added dropwise and the mixture was stirred at room temperature for 4 h. Afterwards, the pH of the mixture was adjusted to 7 with 0.1 mol L^{-1} HCl and the supernatant was collected after standing overnight. The brown AMC powder was finally collected by freeze-drying under vacuum.

Synthesis of Zr-MOF/AMC. AMC (80 mg) was dissolved in 20 mL PBS (pH 7.4). Then 100 mg of 1-ethyl-3-(3-dimethylaminopropyl)carbodiimide and 100 mg of *N*-hydroxysuccinimide were introduced for the activation of the carboxyl groups in AMC. Zr-MOF (40 mg) was added and stirred at room temperature for 8 h. The product Zr-MOF/AMC was washed with deionized water and then the brown colored product was obtained by freeze-drying under vacuum.

2.4 Luminescence properties

The fluorescence properties of MOF, AMC and Zr-MOF/AMC were measured at the excitation wavelength of 380 nm, and all the samples were kept at the same concentration. In order to explore the capability of Zr-MOF/AMC as a fluorescent probe for the determination of GSH, Zr-MOF/AMC (0.1 mL at 2 mg mL^{-1}) was added to GSH solutions of different concentrations (0.001, 0.005, 0.01, 0.05, 0.1, 0.5, 1, 5 and 10 mmol L^{-1}). After the mixtures had been incubated at 37 °C for 3 h, the fluorescence was measured.

The effect of the microenvironment of the cells on the fluorescence of Zr-MOF/AMC was explored. The variations in the fluorescence of AMC in the presence of GSH at different concentrations (0, 1.0 and 10.0 mmol L^{-1}) at pH 5.8 and pH 7.4 were investigated.

2.5 Drug loading and drug release

Zr-MOF/AMC (0.1 g) was dispersed into 20 mL of MTX solution (0.1 g L^{-1}) and stirred for 24 h. The supernatant was then collected and measured by UV-vis spectrophotometry at 300 nm to calculate the MTX drug loading efficiency and drug loading content according to the following equations: $(M_{\text{initial drug}} - M_{\text{drug in supernatant}})/M_{\text{initial drug}} \times 100\%$ and $(M_{\text{initial drug}} - M_{\text{drug in supernatant}})/M_{\text{material}}$.

In order to investigate the pH/GSH dual-responsive release behavior of MTX, samples of the MTX-loaded Zr-MOF/AMC were packaged into dialysis bags (MWCO = 3500), and then each was immersed in 25 mL PBS solution at a given pH (7.4 or 5.8) and GSH concentration (5 mM or 20 mM). At different time points, 3.0 mL solution was removed to determine the concentration of MTX, and then it was replaced with 3.0 mL fresh PBS solution. Three independent experiments were carried out for each condition to obtain the mean value.

2.6 *In vitro* cellular toxicity

All cells were kindly provided by the Stem Cell Bank, Chinese Academy of Sciences. HepG2 and L-02 cells were cultured in standard cell media in 96-well plates and incubated in 5% CO_2 at 37 °C for 24 h. Then different concentrations of particles were added into the 96-well plates and the cells were cultured for a further 24 h. Cell viability was determined using the CKK-8 (2-(2-methoxy-4-nitrophenyl)-3-(4-nitrophenyl)-5-(2,4-disulfophenyl)-2*H*-tetrazolium,monosodium salt) assay. The cells were cultured for 24 h with Zr-MOF/AMC particles (concentrations from 25 to 500 μg mL^{-1}) in a 96-well plate in final volumes of 200 μL with 20 000 cells per well. The cells were then incubated with 100 mL free Zr-MOF/AMC or MTX-loaded Zr-MOF/AMC (concentrations from 25 to 500 μg mL^{-1}) in PBS buffer for 24 h. Cells were rinsed three times with PBS and then 100 μL of 0.1 mg mL^{-1} CKK-8 solution was added to each well and incubated for 30 min at 37 °C. Finally, an ELISA reader was used to measure the absorbance at 380 nm of each well. Results are expressed as the cell viability percentages. Untreated cells in medium were used as controls.

2.7 Intracellular imaging of GSH

In order to further verify the effective sensing of GSH in physiological systems, the imaging capability of Zr-MOF/AMC for the detection of intracellular GSH was assessed. HeLa cells are cultured in 96-well plates with 1×10^4 cells per well for 24 h on 22 × 22 mm glass coverslips in DMEM media at 37 °C in a 5% CO_2 incubator. The cultured cells were washed with phosphate buffer and treated with 0.2 mg mL^{-1} Zr-MOF/AMC for 3 h. As the control experiment, the cells were pre-incubated with 500 mol L^{-1} *N*-ethylmaleimide (NEM, a trapping reagent that acts as a scavenger of thiols) for 30 min to scavenge the thiols in the cells, and then incubated with 0.2 mg mL^{-1} Zr-MOF/AMC in culture medium for 3 h. Finally, the fluorescence images of cells treated and untreated with NEM were obtained by confocal laser scanning microscopy with ex/em at 380/420–440 nm.

3 Results and discussion

3.1 Characterization

Fig. 1(a) shows the powder XRD pattern of the synthesized Zr-MOF; the pattern is in good agreement with that previously reported.[21] The high intensity of the XRD characteristic peaks indicates the highly crystalline structure of the synthesized Zr-MOF. The successful synthesis can also be proved from the FT-IR spectra, as shown in Fig. 1(b). The absorption spectrum of

 This journal is © The Royal Society of Chemistry 2020

Open Access Article. Published on 17 January 2020. Downloaded on 12/9/2025 4:51:02 AM.
This article is licensed under a Creative Commons Attribution-NonCommercial 3.0 Unported Licence.

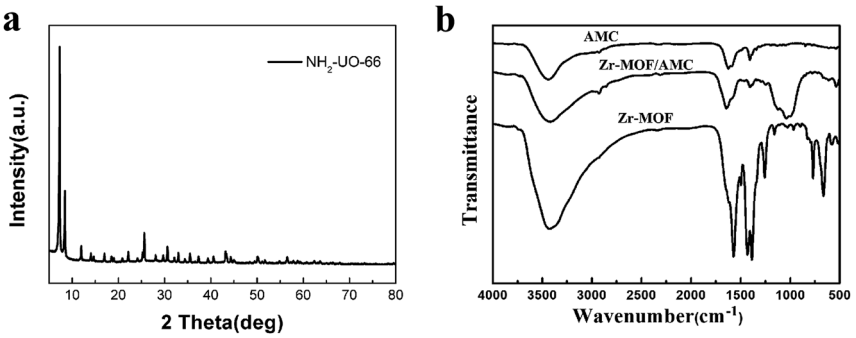

Fig. 1 XRD patterns (a) and FT-IR spectra (b).

Zr-MOF/AMC is similar to that of AMC. The stretching band at 1644 cm^{-1} and the broad band at 3418 cm^{-1} in the spectrum of Zr-MOF/AMC indicate the presence of a –C═O group and an –OH group, respectively. The stretching band at 1590 cm^{-1} can be attributed to the formation of C═N–R (imine) between the acetaldehyde and primary amine group, proving that AMC is grafted onto the surface of Zr-MOF. Since AMC is hybridized on the surface of Zr-MOF, the peaks for the *para*-position and C–H bond in the benzene ring are weakened.

The SEM and TEM images of Zr-MOF and Zr-MOF/AMC are displayed in Fig. 2. Fig. 2(a) shows that the Zr-MOF particles are well dispersed with a uniform size of 200 nm, which can be also seen in Fig. 2(c). The morphology of the composite Zr-MOF/AMC is show in Fig. 2(b) and (d). The surface of the MOF is clearly covered by flocs, but the structure of Zr-MOF is not affected. This indicates that AMC has been successfully coated on the Zr-MOF.

Furthermore, dynamic light scattering (DLS) measurements show that the average diameter of the Zr-MOF nanoparticles is 220 nm (Fig. S1(a)†). The particle size increases from 219 to 231 nm after the formation of Zr-MOF/AMC, meaning that the thickness of the shell is approximately 12 nm.

The composition of the Zr-MOF/AMC is evident from the field emission SEM (FE-SEM) image and EDX elemental mapping data, as shown in Fig. 3. Fig. 3(a) shows that the elements C, N, O and Zr are evenly distributed in Zr-MOF. In addition to all the elements of the Zr-MOF, the Zr-MOF/AMC composite includes the element S originating from the "–S–S–" of AMC, which also proves the successful synthesis of Zr-MOF/AMC. Since the material is coated on a conductive paste during the test (which contains the element C), the distribution area of the C element is slightly different from those of the other elements.

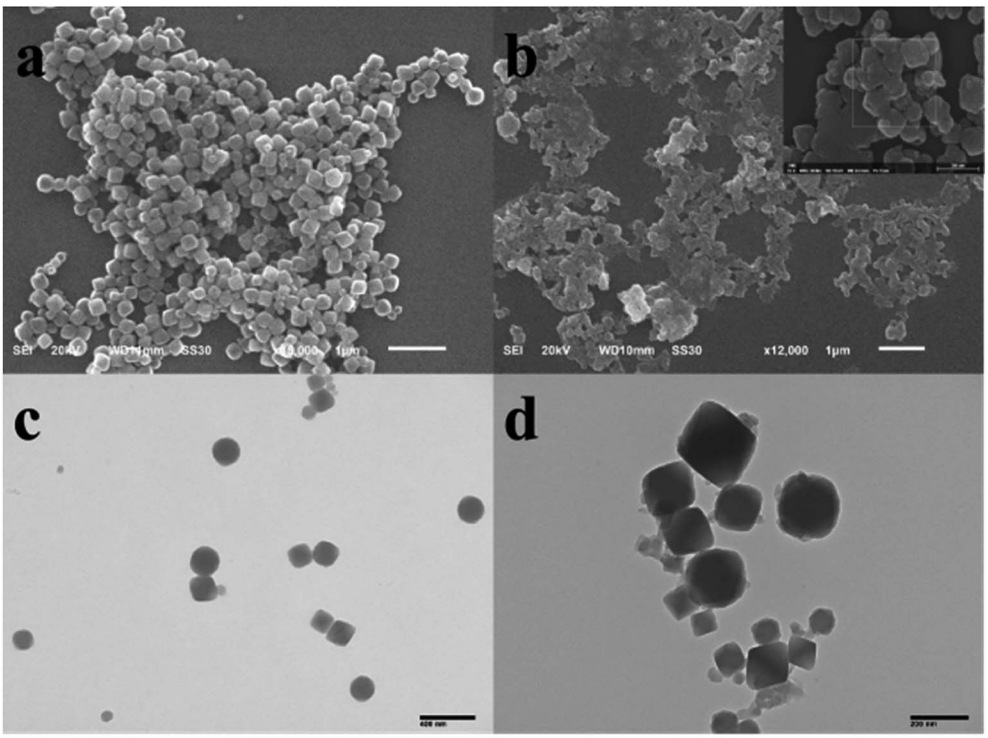

Fig. 2 SEM and TEM images of (a and c) Zr-MOF and (b and d) Zr-MOF/AMC.

Open Access Article. Published on 17 January 2020. Downloaded on 12/9/2025 4:51:02 AM.
This article is licensed under a Creative Commons Attribution-NonCommercial 3.0 Unported Licence.

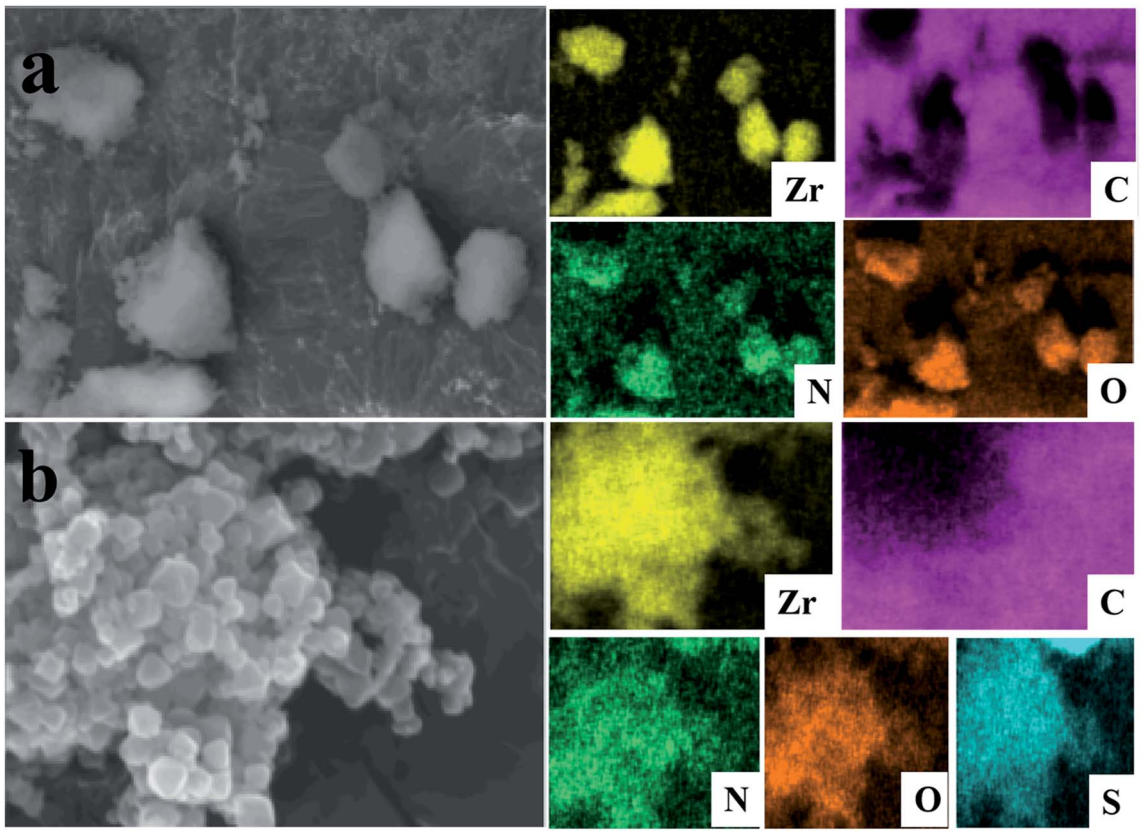

Fig. 3 FE-SEM images and EDX elemental mapping of Zr-MOF (a) and Zr-MOF/AMC (b).

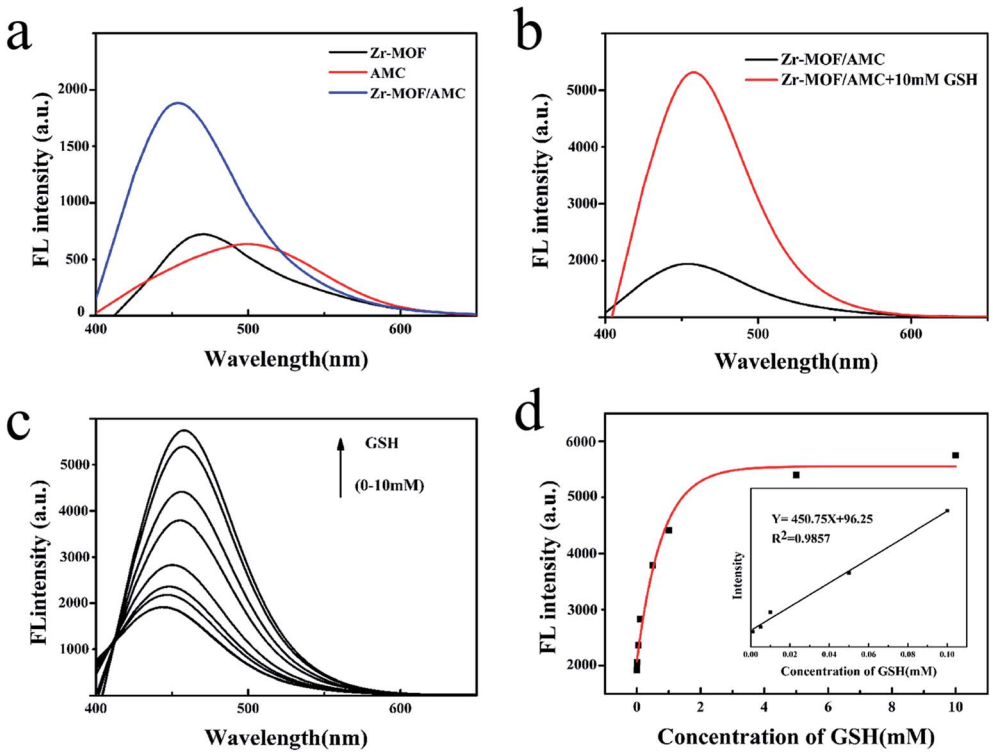

Fig. 4 Fluorescence spectra of Zr-MOF, AMC and Zr-MOF/AMC (a), 0.1 mL Zr-MOF/AMC in 0 mM and 10 mM GSH solution (b), and 0.1 mL Zr-MOF/AMC in the presence of different concentrations of GSH after incubation (c). (d) Concentration-dependence of the Zr-MOF/AMC fluorescence intensity towards GSH (0–10 mmol L^{-1}) and the linear calibration of fluorescence intensity and GSH concentration.

 This journal is © The Royal Society of Chemistry 2020

Open Access Article. Published on 17 January 2020. Downloaded on 12/9/2025 4:51:02 AM.
This article is licensed under a Creative Commons Attribution-NonCommercial 3.0 Unported Licence.

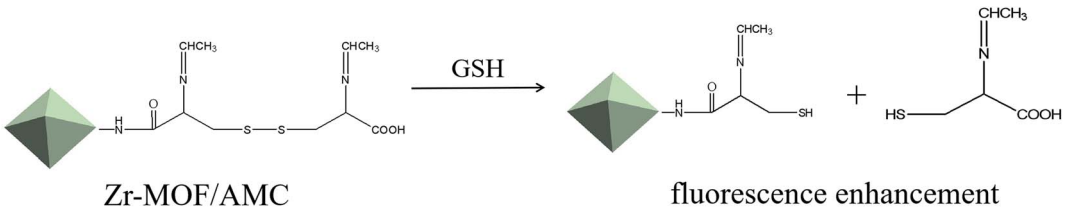

Scheme 2 Schematic illustration of the reaction mechanism of Zr-MOF/AMC in the sensing of GSH.

3.2 Luminescence properties

The fluorescence spectra of Zr-MOF, AMC and Zr-MOF/AMC are shown in Fig. 4(a). Zr-MOF has a fluorescence peak at 475 nm while the fluorescence peak of AMC is at 500 nm. In comparison, the fluorescence intensity of Zr-MOF/AMC is obviously enhanced and the fluorescence peak is blue-shifted to 450 nm, which can be explained by an intermolecular effect.

In order to explore the potential of using Zr-MOF/AMC as a probe for GSH detection, the effect of GSH on the fluorescence of Zr-MOF/AMC was investigated. Fig. 4(b) shows that the fluorescence intensity significantly increases with the addition of GSH. When the disulfide bond in AMC is exposed to the glutathione microenvironment, a thiol–disulfide exchange reaction occurs between the disulfide bond and glutathione, resulting in the cleavage of the –S–S– bond into thiols (–SH) to produce two fluorescent molecules, as shown in Scheme 2. The fluorescence intensity is remarkably enhanced as the two fluorescent molecules diffuse.

To prove that the Zr-MOF/AMC can be used to quantitatively detect GSH, the effect of different concentrations of GSH on the fluorescence of Zr-MOF/AMC was examined, as shown in Fig. 4(c). With increasing concentration of GSH, the fluorescence intensity gradually increases. The intensity is proportional to the concentration of GSH, as shown in Fig. 4(d). The relation between the fluorescence intensity and GSH concentration follows the polynomial function $F = -174e(-C/0.78) + 278$ within a concentration range of 0–10.0 mmol L^{-1} GSH. A linear calibration curve can be obtained in the concentration range of 0–0.1 mM L^{-1} GSH. The linear equation is $F = 450.75C + 96.25$ and the limit of detection is 4.624 μmol L^{-1} (3δ/k, $n = 9$), where δ is the standard deviation of the blank measurement and k is slope. This limit of detection is lower than those of most GSH detection probes.[16] Therefore, Zr-MOF/AMC can be used in the quantitative determination of GSH.

For the purpose of demonstrating the potential applications of Zr-MOF/AMC in GSH sensing in cancer cells, where the pH value generally varies significantly, the fluorescence of Zr-MOF/AMC was investigated at pH 5.8 and 7.4, as shown in Fig. 5. The fluorescence of the Zr-MOF/AMC depends on the concentration of GSH, and pH has no effect. This provides good proof of the suitability of Zr-MOF/AMC as a probe for detecting the GSH concentration in biological environments.

3.3 Drug-loading and release behavior

MTX was selected as a drug model, and it could be loaded on the Zr-MOF/AMC nanocarrier to produce a Zr-MOF/AMC/MTX conjugate, mainly *via* electrostatic interactions with the –COOH groups on AMC and adsorption interactions with Zr-MOF. The drug loading for MTX was 36 mg g^{-1}.

The pH of cells in the tumor microenvironment (pH < 6.8) is lower than that of normal cells (pH ~ 7.4). It is worth noting that the pH values of the endosomal and lysosomal compartments may be as low as 5.5–6.0 and 4.5–5.0, respectively.[22,23] Moreover, the GSH concentration in normal cells is about 5 mM, and the concentration in cancer cells is about four times

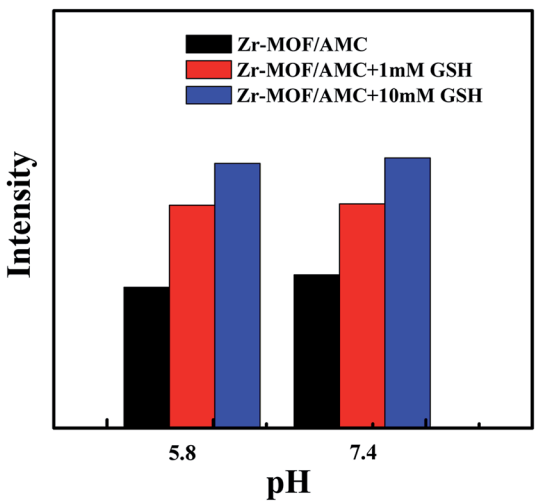

Fig. 5 Fluorescence variation of Zr-MOF/AMC (0.2 mg mL^{-1}) in the presence of GSH (0, 1.0, 10.0 mmol L^{-1}) at pH 5.8 and 7.4.

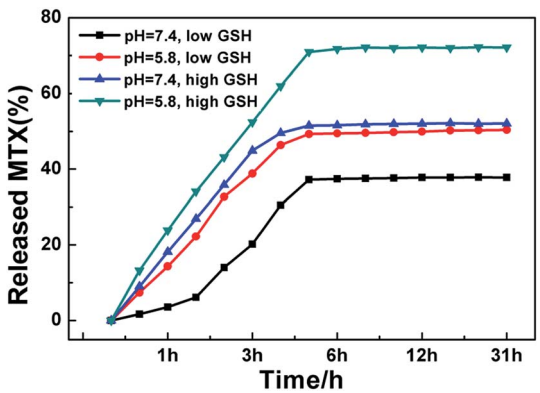

Fig. 6 MTX release profiles from Zr-MOF/AMC at different pH values and different concentrations of GSH.

Open Access Article. Published on 17 January 2020. Downloaded on 12/9/2025 4:51:02 AM.
This article is licensed under a Creative Commons Attribution-NonCommercial 3.0 Unported Licence.

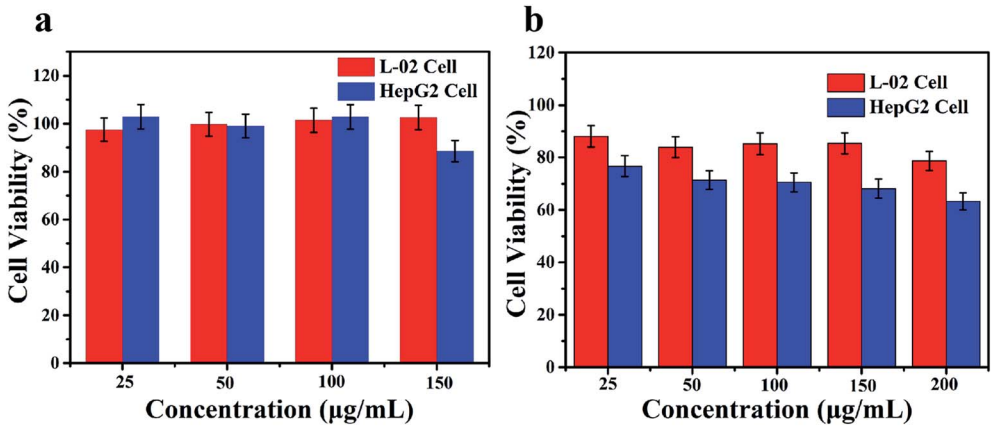

Fig. 7 The cytotoxicities of Zr-MOF/AMC (a) and Zr-MOF/AMC/MTX (b) in HepG2 liver cancer cells and L-02 normal liver cells. Error bars represent standard deviations obtained from three measurements.

that of normal cells. Therefore, the MTX release behaviors at different pH values (pH 7.4 and pH 5.8) and different concentrations of GSH (5 mM and 20 mM) were tested to evaluate the microenvironment-responsive release of MTX from Zr-MOF/AMC; the results are shown in Fig. 6.

Fig. 6 illustrates that at the same GSH concentration, the drug release at pH 5.8 is higher than that at pH 7.4. Under acidic conditions, the –C═N bond in AMC hydrolyzes or partly cleaves, causing MTX to fall off the carrier. It can also be seen that at the same pH value, the drug release at the high GSH concentration (20 mM) is higher than that at the low GSH concentration (5 mM). At high concentration, GSH cleaves the –S–S– bond of AMC and reduces the integrity of the Zr-MOF/AMC, triggering the release of the loaded MTX from the nanocarrier.[24,25] These results prove that Zr-MOF/AMC can be used for pH/GSH dual-responsive drug delivery. It is clear that the MTX release reaches 75% at pH 5.8 and high concentration GSH (tumor cell environment), while the release is 32% at pH 7.4 and low concentration GSH (normal cell environment). The pH/GSH dual-responsive release can help deliver drugs to cancer cells more precisely.

3.4 *In vitro* cytotoxicity

To investigate the intracellular microenvironment-targeted drug release of Zr-MOF/AMC, cytotoxicity experiments were performed. HepG2 cells (human hepatoma cells) and L-02 cells (normal hepatocyte cells) were used to represent cancer cells

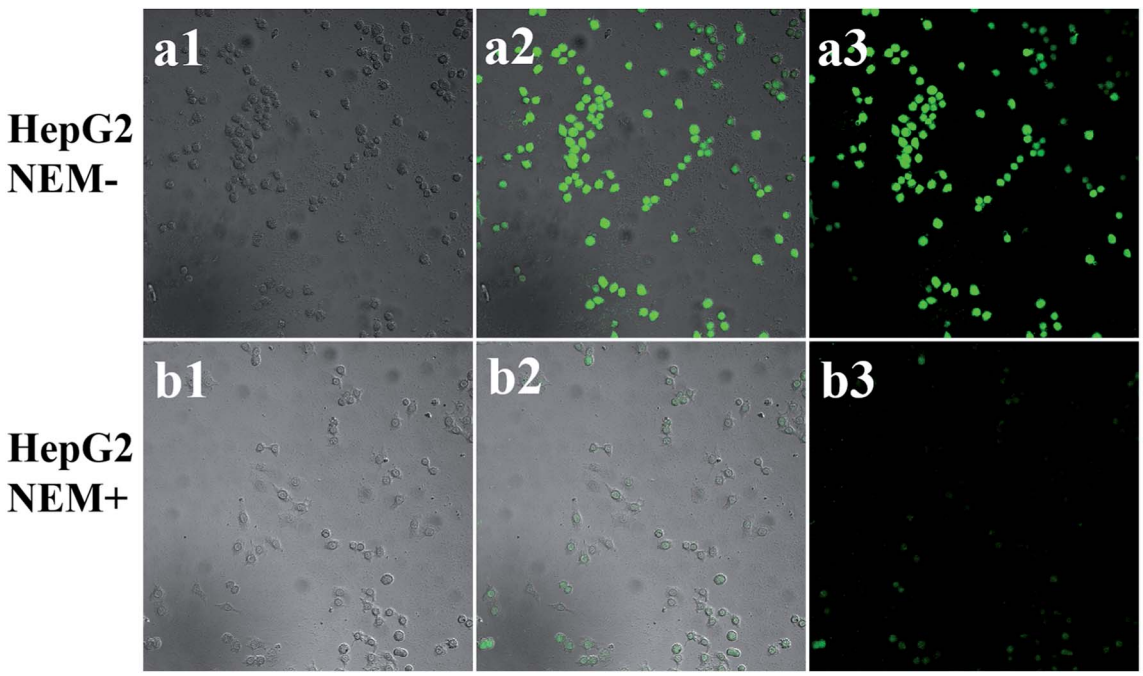

Fig. 8 Confocal fluorescence images of HepG2 cells. (a1–a3) Cells that have been incubated with 0.2 mg mL^{-1} Zr-MOF/AMC for 3 h; (b1–b3) cells that have been pretreated with 500 μmol L^{-1} NEM for 30 min, before incubation with 0.2 mg mL^{-1} Zr-MOF/AMC for 3 h. The green fluorescence is recorded at $\lambda_{ex}/\lambda_{em}$ = 380/440–480 nm.

 This journal is © The Royal Society of Chemistry 2020

Open Access Article. Published on 17 January 2020. Downloaded on 12/9/2025 4:51:02 AM.
This article is licensed under a Creative Commons Attribution-NonCommercial 3.0 Unported Licence.

and normal cells, respectively. The cell viabilities of HepG2 cells and L-02 cells after incubation with different concentrations of Zr-MOF/AMC and MTX-loaded Zr-MOF/AMC are shown in Fig. 7. It can be seen from Fig. 7(a) that the survival rates of both cells incubated with 150 μg mL^{-1} of Zr-MOF/AMC are above 80%, demonstrating the low cytotoxicity and good biocompatibility of Zr-MOF/AMC. It is worth mentioning that the cell viabilities of HepG2 and L-02 are different after incubation with Zr-MOF/AMC/MTX. The survival rate of L-02 cells incubated with 200 μg mL^{-1} of Zr-MOF/AMC/MTX is still above 80%, indicating that little MTX is released in normal cells. In contrast, the survival rate of HepG2 cells is 76% after incubation with only 25 μg mL^{-1} of Zr-MOF/AMC/MTX, and 63% with 200 μg mL^{-1} of Zr-MOF/AMC/MTX, as shown in Fig. 7(b). The enhanced cytotoxicity in HepG2 cells of MTX-loaded Zr-MOF/AMC is due to the endocytosis-mediated intercellular drug delivery through the nanocarriers.[26,27] This shows that Zr-MOF/AMC is passively targeted and is easily enriched in cancer cells, resulting in a greater release of the loaded MTX in cancer cells than in normal cells. Due to the pH/GSH dual response of the drug carrier and the special microenvironment of cancer cells, Zr-MOF/AMC shows reduced toxicity to normal cells and thus will have reduced side effects.

3.5 Intracellular GSH imaging

In order to explore the capability of Zr-MOF/AMC as a probe for identifying the abnormal GSH concentration of cancer cells, HepG2 cells were used for GSH imaging. For further assessing the capability of Zr-MOF/AMC for the selective visualization of GSH in living cells, HepG2 cells were first pretreated with 500 μmol L^{-1} of NEM for 30 min to reduce the intracellular concentration of GSH where NEM serves as a thiol scavenger.[28,29] As shown in Fig. 8(b1–b3), a weak fluorescence signal is observed for NEM-treated HepG2 cells, owing to the reduction of GSH concentration. In contrast, untreated HepG2 cells exhibit a stronger green fluorescence, as shown in Fig. 8(a1–a3), indicating that Zr-MOF/AMC can be used to selectively visualize GSH in living cells, on the basis of the reaction between Zr-MOF/AMC and the abundant GSH in HepG2 cells. It therefore provides a tool for cancer cell discrimination.

4 Conclusions

In summary, the hybrid Zr-MOF/AMC/MTX was successfully synthesized through functionalization of the surface of Zr-MOF with acetaldehyde-modified cystine (AMC). As the –S–S– and –C═N– bonds in AMC change with high GSH concentrations and acidic conditions, the hybrid can be used for pH/GSH dual-responsive drug delivery. Due to the cleavage of the –S–S– bonds, the AMC on the surface of Zr-MOF/AMC/MTX is split into two fluorescent molecules, so producing strong fluorescence which can be used to quantitatively detect GSH. Therefore, the design of Zr-MOF/AMC/MTX illustrates a new synthetic approach for the construction of drug carriers for integrated diagnosis and treatment.

Conflicts of interest

There are no conflicts to declare.

Acknowledgements

This work was supported by the Natural Science Foundation of Hubei Province (No. 2017CFB530), Wuhan Morning Light Plan of Youth Science and Technology (No. 2017050304010282) and the National Natural Science Foundation of China (No. 51302071). The cytotoxicity and cell imaging tests were performed at Wuhan Bioeagle Biological Technology Co., Ltd.

References

1 B. Lei, M. Wang and Z. Jinag, *ACS Appl. Mater. Interfaces*, 2018, **10**, 16698.
2 L. Y. Niu, Y. Z. Chen and H. R. Zheng, *Chem. Soc. Rev.*, 2015, **44**, 6143.
3 X. Zhang, F. G. Wu and P. Liu, *Small*, 2015, **10**, 5170.
4 H. S. Jung, X. Chen, J. S. Kim and J. Yoon, *Chem. Soc. Rev.*, 2013, **42**, 6019.
5 W. A. Kleinman and J. P. Richie, *Biochem. Pharmacol.*, 2000, **60**, 19–29.
6 D. M. Townsend, K. D. Tew and H. Tapiero, *Biomed. Pharmacother.*, 2003, **57**, 145.
7 Y. Shi, Y. Pan and H. Zhang, *Biosens. Bioelectron.*, 2014, **56**, 39.
8 G. Fei, C. Liang and Y. Nailin, *Nano Lett.*, 2018, **9**, 6037.
9 W. Zhang, J. H. Mao and W. Zhu, *Nat. Commun.*, 2016, **7**, 12619.
10 P. Zhang, Y. Wang and J. Lian, *Adv. Mater.*, 2017, **29**, 1072.
11 W. Shunzhi, L. Yijun and O. K. Farha, *Chem. Mater.*, 2018, **30**, 4877.
12 S. Wuttke, A. Escudero and B. Rungtaweevoranit, *Biomaterials*, 2017, **123**, 172.
13 R. Freund, U. Lächelt and B. Rühle, *ACS Nano*, 2018, **12**, 2094.
14 P. Horcajada, T. Chalati and C. Serre, *Nat. Mater.*, 2009, **9**, 172–178.
15 Y. Jia, Y. Cui and J. Fei, *Adv. Funct. Mater.*, 2012, **22**, 1446.
16 L. Hu, X. Wei and J. Meng, *Sens. Actuators, B*, 2018, **268**, 264.
17 H. Zeng, Z. S. Chen and M. G. Belinsky, *Cancer Res.*, 2001, **61**, 7225.
18 H. L. Min, Z. Yang and C. W. Lim, *Chem. Rev.*, 2013, **113**, 5071.
19 Y. Xin and J. Yuan, *Polym. Chem.*, 2012, **3**, 3045.
20 H. Molavi, A. Shojaei and A. Mousavi, *J. Mater. Chem. A*, 2018, **6**, 2775.
21 X. Wang, X. Zhao and D. Zhang, *Appl. Catal., B*, 2018, **228**, 47.
22 J. Hao, F. Liu and N. Liu, *Sens. Actuators, B*, 2017, **245**, 641.
23 N. Xiao, H. Liang and J. Lu, *Soft Matter*, 2011, **7**, 10834.
24 Y. Jia, J. Fei and Y. Cui, *Chem. Commun.*, 2011, **47**, 1175.
25 R. Franco and J. A. Cidlowski, *Cell Death Differ.*, 2009, **16**, 1303.
26 A. N. Koo, H. J. Lee and S. E. Kim, *Chem. Commun.*, 2008, 6570.
27 Y. Chen, K. Ai and J. Liu, *Biomaterials*, 2015, **60**, 111.
28 X. L. Zhang, C. Zheng and S. S. Guo, *Anal. Chem.*, 2014, **86**, 3426.
29 L. M. Shen, Q. Chen and Z. Y. Sun, *Anal. Chem.*, 2014, **86**, 5002.